Sigma Journal of Engineering and Natural Sciences
Web page info: https://sigma.yildiz.edu.tr
DOI: 10.14744/sigma.2024.00003

Research Article

Nanoscale detection of ovarian cancer biomarker

Marwah AL-OGAIDI[1,*], Nuha NIHAD A. ABURAHMA[2], Ansam M. SALMAN[1], Haider RAAD[3]

[1]Department of Laser and Optoelectronics Engineering, Al-Nahrain University, Baghdad, 10072, Iraq
[2]Department of Chemistry, College of Science, University of Baghdad, Baghdad, 10071, Iraq
[3]Department of Physics and Engineering, Xavier University, Cincinnati, Ohio, 45207, USA

ARTICLE INFO

Article history
Received: 04 September 2023
Revised: 25 November 2023
Accepted: 02 January 2024

Keywords:
Cancer Serum Antigen (CA-125); Ovarian Cancer; Quantum dots (QDs)

ABSTRACT

It is estimated that over 2,000 women globally are impacted by ovarian cancer (OC). Unfortunately, every year, over half of the cases end in death. This underscores the critical importance of better early detection and diagnosis of OC. Research into improving a sensitive, dependable, and rapid cancer serum antigen (CA-125) detector is essential for medical diagnosis. This antigen may signal the earliest stages of ovarian cancer. The typical crystalline size of the Cadmium selenide (CdSe) quantum dots (QDs) that we synthesized and coated is adjusted in this study to be 8 ± 0.2 nm. Multiple characterization methods, including X-ray diffraction, Z-scan, and transmission electron microscopy, were utilized to verify their properties. We used these QDs as optical tags for a sandwich assay, which was used to test a high-binding surface where the capture antibody was immobilized. Popular optical tags (QDs), semiconductor nanoparticles with size-dependent fluorescence spectra, brightness, and photostability, were used and can be detected by a microplate spectrophotometer. A linear curve was observed within a range of 5–1000 U/ml CA-125, which is suitable for quantitative work, and the detection limit was 4.5 U/ml. The interference with the detection of CA-125 was tested in human serum, and the results showed no significant difference in the fluorescence spectra. Third-order nonlinear optical parameter analysis of conjugated CdSe QDs under an excitation beam power level of approximately 120 W and a wavelength of 532 nm was determined in detail. The third-order optical susceptibility ($\chi 3$) was 2.746×10^{-7} esu with a sound absorption coefficient of 4.68556×10^{-5} cm/W and nonlinear refractive index -5.6132×10^{-9} cm^2/W. Finally, the resulting CdSe QDs have been effectively employed in the labeling and, hence, detection of ovarian cancer antigen (CA-125).

Cite this article as: Al-Ogaidi M, Nihad A. Aburahma N, Salman AM, Raad H. Nanoscale detection of ovarian cancer biomarker. Sigma J Eng Nat Sci 2024;42(6):1884–1891.

***Corresponding author.**
*E-mail address: marwah.a.zaidan@nahrainuniv.edu.iq

This paper was recommended for publication in revised form by Editor-in-Chief Ahmet Selim Dalkilic

INTRODUCTION

Among Western women infected with cancer, ovarian cancer (OC) is the seventh foremost cause of mortality [1, 2]. Worldwide, OC affects 239,000 females. More than half of all cases end in death each year, and the rates of new cases and deaths among women with OC have remained consistent since 1992 [3]. The origin of the anomalous cells in the ovarian tissue helps to classify the various forms of OC. Epithelial carcinoma encompasses most newly diagnosed cases, specifically around 90% [4]. Discomfort during eating, gas, and abdominal pain are typical signs of OC. However, these symptoms cannot be utilized as a sole diagnostic tool for OC because they are present in the general female population without OC [5]. This is why OC is sometimes called the "Silent Killer" [6]: it is not detectable until the disease has progressed significantly. Computed tomography (CT) scans of the chest, abdomen, and pelvis, pelvic examination, and transvaginal ultrasound are used to assess the extent to which the disease has spread beyond the pelvic area, even when OC is presumed [7]. To determine the stage of OC, conducting procedures like colonoscopy, laparoscopy, and biopsy is necessary. However, patients may experience discomfort during and after these procedures [8]. Even though various forms of OC involve genetic and epigenetic alterations, the currently licensed tests for disease identification, such as cancer detection and monitoring, are protein-based assays [9].

Bast et al. (1983) described cancer antigen serum (CA-125) as an additional helpful tool alongside radiological and imaging testing. They documented this glycoprotein type using the mAb OC 125. In 80% to 85% of women diagnosed with epithelial OC, CA-125 levels in the bloodstream rose. Several follow-up investigations have shown the association between an elevated CA-125 level and ovarian cancer. A high CA-125 level usually indicates late-stage OC, but in early-stage OC, less than half of the cases showed an elevated level of this marker. CA-125 is a significant tumor marker. Other types of cancers, including colon, pleura, breast, peritoneum, pancreas, Müllerian epithelial cells, and pericardium, have been associated with higher levels of CA-125, according to other research [11,12]. It has been accepted to test for OC using CA-125 in conjunction with a physical examination [13,14]. The effectiveness of OC diagnosis has been the target of intensive attempts to validate individual indicators [15].

An important area of research that could significantly affect the care and outcomes of ovarian cancer is the development of a biosensor for early diagnosis. In many cases, the sensitivity and specificity of the existing procedures used to diagnose OC are inadequate, resulting in diagnoses made at a late stage and low survival rates. As a result, we announce the creation of a trustworthy and sensitive technique for detecting low CA-125 concentrations, which may show early phases of OC; this could lead to a paradigm shift in the field and better patient outcomes. The size-dependent fluorescence spectra, photostability, brightness, and detectability by fluorescence spectrophotometry of optical quantum dot (QD) tags—constructed of semiconductor nanoparticles (NPs)—have contributed to their rising popularity.

Perspectives

The advent of nanotechnology may drastically alter the diagnosis, treatment, and prevention of numerous diseases, including cancer [16-20]. A semiconductor core plus a secondary semiconductor material form the nanocrystals known as quantum dots (QDs). The core can have a diameter anywhere from 2 nm to 10 nm. The optical and electronic features for QDs are distinct from those of organic dyes and fluorescent proteins. These properties include controlling light emission depending on size and composition, increasing signal brightness, resistance to photobleaching, and stimulating numerous fluorescence colors simultaneously [21-25].

Using QDs for bioimaging and cancer diagnostics is rapidly expanding in cancer research. In a perfect world, QD-based probes would be used for the early detection and noninvasive treatment of both primary and metastatic malignancies. The development of quantum dot (QD) probes endowed with enhanced target selectivity, signal intensity, and therapeutic potential—all while mitigating cytotoxicity and nonspecificity—is imperative, as existing electrochemical biosensors and their applications remain in their infancy. An integrated platform is required before its extensive use in cancer diagnosis and treatment to simplify detection and enhance automation. Solubilizing QDs before their application requires surface modification with biofunctional compounds [26]. Diagnosing and treating cancer with high specificity is possible with diagnostic and therapeutic agents [27-29].

There has been a lot of interest in QDs for active targeting of cancer antigens because of their potential use in early cancer imaging and diagnostics [30-32]. Yet, there are still obstacles to overcome before clinical applications may be achieved, such as improving sensitivity, increasing specificity, and decreasing QD toxicity. If QD-based nanotechnology is to make significant strides in cancer treatment, researchers and experts from many domains must work together. Reported studies in this field are explained in Table 1.

GENERAL PROCEDURE

Chemicals and Materials

There was no further sterilization of the substances utilized in the research. Sigma-Aldrich (St. Louis, MO) supplied the CA-125 antigen, anti-mouse CA-125 detection Ab IgG1, PBS-Tween 20, HCl, sulfo-NHS, and Ethylene dichloride (EDC). A Millipore Milli-Q filtration system produced pure deionized water to prepare aqueous solutions. A black

Table 1. Reported studies in the field of QDs

Researchers' names	Category of QDs	Major Findings	Advantages	Problems
Tada *et al.,* 2007, [33].	Trastuzum Ab-QDs (800 nm)	Using quantum dots, one breast cancer cell may be seen.	Superb light output; photobleaching resistance.	Intracellular delivery technologies, as they stand, need to be improved.
Shah *et al.,* 2007, [34].	Bioconjugated QDs	During multiline age differentiation and stem cell proliferation, QDs can efficiently label cells for an extended period.	InP/ZnS QDs are nontoxic.	Due to the reaction environment sensitivity of precursors and surfactants, generating desirable InP/ZnS QDs is challenging.
Yong *et al.,*2009, [35].	Bioconjugated InP/ZnS QDs	Non-Cd-based optical imaging nanoprobes made of InP/ZnS QDs are safe and effective.		
Fang, Peng, Pang, & Li, 2012, [36].	QDs	Possible uses for QDs in cancer research include primary tumor detection in vitro, tumor imaging in vivo, invasion study of tumor microenvironment, imaging of progression and multimodality biomedical molecular targeting, and other similar uses.	Unique characteristics of QDs, including fluorescence capacity, make them suitable for cancer theranostic applications.	QDs must be reliably and efficiently guided to a target organ or disease site to maximize their usefulness in biomedicine while avoiding unwanted changes.
Xu & Chen, 2023, [37]	Semiconductor QDs (SQDs)	SQDs can be synthesized using various methods and modified for cancer cell imaging.	It provides better resolution and contrast than traditional clinical cancer imaging methods, such as X-ray CT and magnetic resonance imaging. Targeting molecules to their surface can be directed to specific organs or disease sites.	Cytotoxicity and potential toxicity concerns.
Kumar, Singh, & Singh, 2021, [38]	QDs	QDs have potential applications in cancer theranostics when conjugated with macromolecules.	Unique characteristics of QDs, including fluorescence capacity, make them suitable for cancer theranostic applications.	Potential toxicity concerns.

96-well plate from Fisher Scientific, CdSe core QDs from NNCrystal, octadecylamine (ODA), and 1-octadecene (ODE) were among the other ingredients used.

Preparation and Bioconjugation of Core/Multishell QDs

Here is how multishell quantum dots were made utilizing the sequential ion layer adsorption and reaction technique [18]: In a 100 ml flask, 1.3×10^{-6} mol pure CdSe core QDs, 30 g ODE, and 10.0 g ODA were loaded, nitrogen-filled, and heated on a mantle to 120 °C for 15 min.

Characterization

The X-ray diffractometer (XRD-6000, Shimadzu, Japan) and Cu(k) radiation were used to measure the

crystalline structure of the QD NP. The parameters used were a scanning speed of 5°/min, a wavelength of 1.5405, 60 kV, and 80 mA. The scanning range was 2°, from 20° to 80°. To find out how big and round the QDs were, researchers used a transmission electron microscope (TEM; Philips Holand). Before taking micrographs at a voltage of up to 120 kV (type CM120), a carbon-coated copper grid was used to load a drop of aqueous CdSe QD sample into the transmission electron microscope (TEM). The sample was then let to dry at ambient temperature. Spectrophotometry for linear transmissions and Z-scan for nonlinear transmissions was also investigated. The Z-scan method was accomplished using a second harmonic generation Nd: YAG laser with a Gaussian profile and a beam divergence of 0.711 mrad. The laser excitation power could not exceed 120 W, and the beam diameter had to be less than 1.5 mm. The synthetic sample was moved along the laser axis using a linear translation stage and a convex lens with a 20 cm focal length to study the changes in laser beam intensity. Open- and closed-aperture configurations were adopted to control the nonlinear refraction index (n_2) and absorption coefficient (β).

The 3rd-order nonlinear optical susceptibility $\chi^{(3)}$ can be computed once the n_2 and β have been obtained.

Labeling of CA-125 Detection AB with QDS

CA-125 detection Antibody- Quantum dot (Ab-QD) conjugates were prepared via covalent coupling using sulfo-NHS and EDC. QDs (0.033 µM) with surface carboxyl groups were activated by incubation with sulfo-NHS and EDC for 5 min at pH 7.4. The following step was to add 50 µl of 125 µg/ml CA-125 Ab, mix thoroughly by vortexing, and let it react at room temperature for 2 hours. Two hours later, 2 µl of quenching buffer was added to a reaction, and it was stirred for ten minutes to stop the reaction. After being kept at 4 °C for around 12 hours, the CA-125 Ab QD conjugates were spun in a centrifuge to eliminate unconjugated particles.

Coating of the High-Binding Plate with CA-125 Capture AB

Physical adsorption was used to perform Ab coating. The wells were subjected to a 24-hour treatment with Phosphate buffered saline (PBS) at pH 7.4. Then, the microtiter plate wells were coated with 2 µg/ml Ab solution by pipetting 50 µl diluted Ab in the top wells of the plate. Next, the plate was wrapped and then stored for 12–24 h in a refrigerator at 4 °C. After the removal of the coating solution, the plate was rinsed thrice with 200 µl 10 mM PBS (pH 7.4). The solution was removed by flipping the plate over a sink. The residual droplets were eliminated by gently tapping the plate onto an absorbent paper surface.

Optimization of the Concentrations of Capture and Detection ABS

The concentrations of captured and detected Abs were confirmed. The experiments were performed by fixing all the experimental parameters except the concentration of the capture and detection Abs separately. The capture and detection Abs were tested in 2–20 and 5–100 g/ml, respectively.

Dynamic Range and Standard Calibration Curve

The experiment was conducted in a physiological buffer using identified concentrations of the typical sample (5, 50, 100, 200, 1000, and 5000 U mL^{-1}) to determine the best concentration range for capturing and detecting antibodies.

The experiment used capture and detection antibodies at 2 Ug mL-1 and 5 Ug mL-1, respectively. Each well's optical density was measured at 620 nm to determine the linear range. Triplicate runs of the test were carried out according to the specified linear range. For known antigen concentrations in the existence of biological matrix, the relative signals were determined by establishing the calibration curves.

Testing in the Existence of Human Serum

Following the confirmation of the modifications of Abs, the test was conducted with 50% human serum. The potential for interference from human serum was tested in the assay. In interference tests, the presence or absence of an antigen is tested by adding human serum to a certain amount of the antigen.

RESULTS AND DISCUSSION

The crystal domain size was determined using Gaussian fit on X-ray diffraction (XRD) patterns, employing the Debye-Scherrer formula: $D = 0.9\ \lambda/\beta\ \cos\theta$. Here, ($D$) represents a crystallite mean size, (λ) stands for a wavelength for the incident X-ray (1.5406 Å), θ is the diffraction peak angle, and β is the full width at half maximum of the XRD peak at angle θ. The crystal domain size for CdSe was approximately 6 nm, based on the hexagonal (wurtzite) CdSe structure planes (Figure 1).

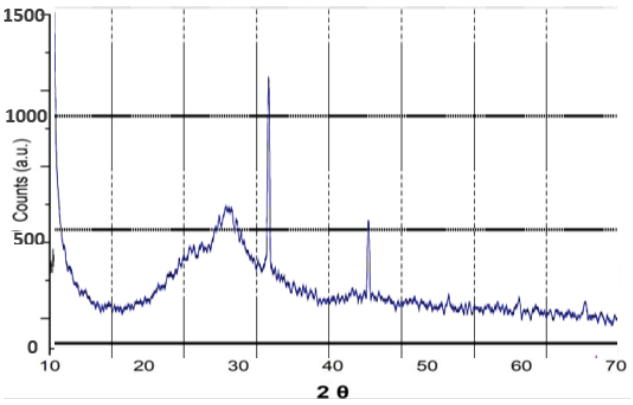

Figure 1. XRD patterns of QDs.

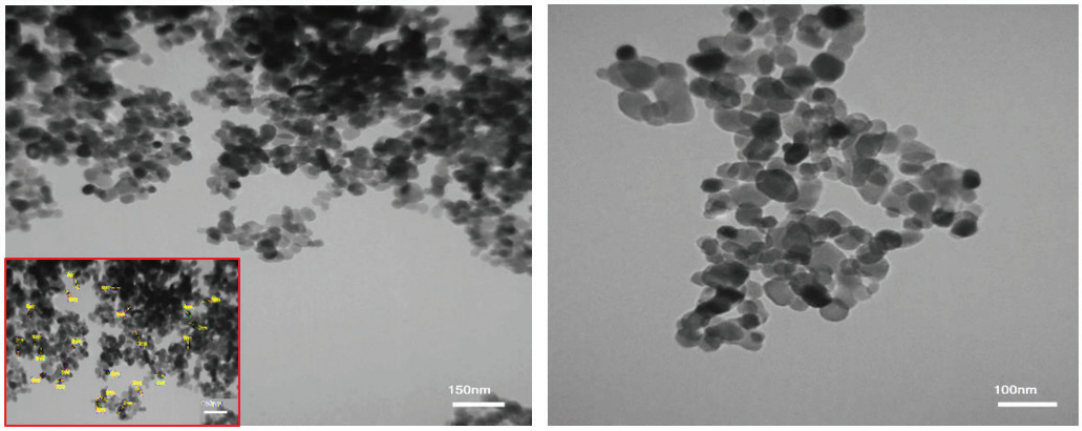

(a) (b)

Figure 2. TEM images of spherical and monodispersed CdSe QDs.

To regulate the actual size and outline of the QDs, we obtained the TEM images of the CdSe QDs (Figure 2). The images demonstrated that the QDs were spherical and had a uniform size distribution of approximately 6 nm.

Figures 2(A) and 2(B) show the TEM micrographs of QDs, further confirming those of the XRD analysis. Micrographs of CdSe QDs exhibited spherical and monodispersed particles with a size of approximately 8 ± 0.2 nm after conjugation with CA-125.

To determine the optical properties of materials (nonlinear refractive index and third nonlinear coefficient) of relatively thin materials, the Z-scan is commonly used in nonlinear optics to assess the nonlinearities of these materials through the calibration of reference samples, as shown in Figure (3). Figures 4(A) and 4(B) show the behavior of the open- and closed-aperture Z-scans. Based on these graphs, the generated sample displayed various nonlinear properties, such as self-defocusing, non-saturable absorption, and two-photon absorption. The normalized charts were fitted with the following equations to estimate the nonlinear parameters:

The nonlinear absorption coefficient (β) was estimated by fitting .[39][40]:

$$T(Z) = \sum_{m}^{2} \frac{\left(\beta I_0 L_{eff} \Big/ 1+\left(\frac{Z}{Z_0}\right)^2 \right)^m}{(m+1)^{3/2}} \quad (1)$$

The nonlinear refractive index (n_2) was obtained as follows .[39][40]:

$$n_2 = \frac{\Delta \emptyset_0}{k I_0 L_{eff}} \quad (2)$$

Where Z_0 denotes the diffraction length (or Rayleigh length) of the beam, I0 represents the laser beam intensity at the focus point (Z=0), Leff stands for an effective propagation length inside a sample, given by Leff=. [(1-exp(-α0 L))/α0], L stands for a geometrical thickness of the prepared sample, m stands for an order for multiphoton processes, k corresponds to the wavenumber (k=2π/λ), and ΔØ0 is a phase shift, specified by |ΔØ0 |=(ΔT(p-v))/(0.406[(1-ST)]^0.25). ST signifies the linear transmittance of the aperture, and ΔT(p-v) and ΔT specify a difference in transmittance between the maximum and minimum magnitudes for closed and open apertures, respectively. The 3rd nonlinear coefficient $\chi^{(3)}$ was estimated using the given relation [39,40]:

$$\chi^{(3)} = \sqrt{(Re\chi^{(3)})^2 + (Im\chi^{(3)})^2} \quad (3)$$

Where the real part is $Re\ (\chi^{(3)}) = 10^{-4} \frac{\varepsilon_0 c^2 n_0^2 n_2}{\pi}$, and the imaginary part is $Im\ (\chi^{(3)}) = 10^{-2} \frac{\varepsilon_0 c^2 n_0^2 \lambda \beta}{4\pi^2}$.

From this experiment, the prepared sample possessed a good β = 4.68556 × 10^{-5} cm/W, n_2 = -5.6132 × 10^{-9} cm^2/W, and a high $\chi^{(3)}$ = 2.746 × 10^{-7}.

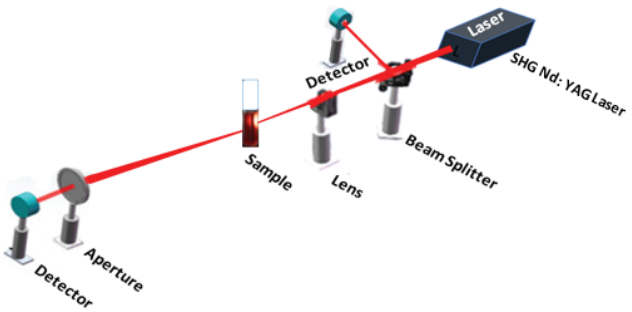

Figure 3. Setup for Z-scan.

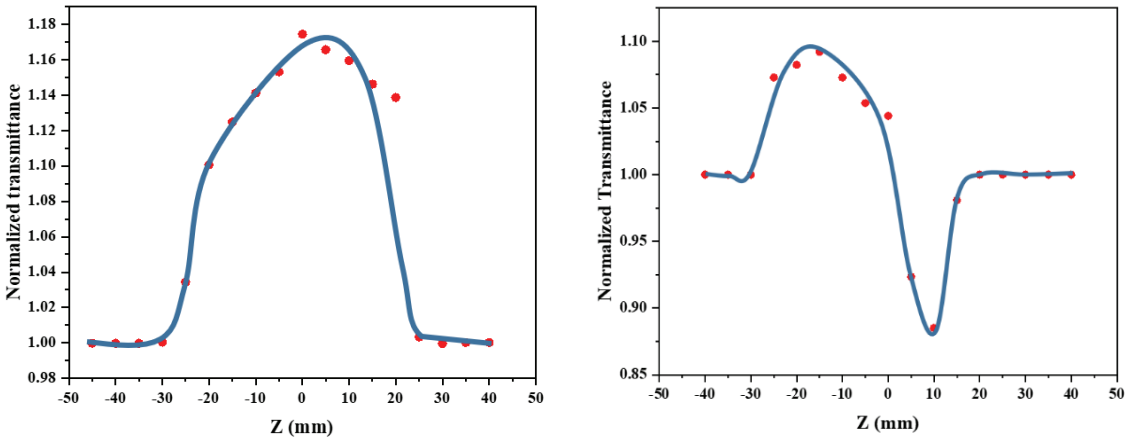

(a) (b)

Figure 4. Normalized transmission in (a) open- and (b) closed-aperture conditions.

Optimization of ABS

In the current study, sandwich-type immunoreactions were performed on 96-well plates to detect protein, and this approach yielded good sensitivity and specificity .[41]. In general, the high concentration of any of the captured or detected Abs caused nonspecific adsorption of the conjugates, which led to a high background signal. Under our experimental conditions, 2 and 5 μg/ml monoclonal capture and detection of Abs were confirmed, respectively.

The findings on fluorescence intensity in correlation with the antigen concentrations are comparable with [42].

Analytical Performance

The quantitative detection of the analyte was achieved by measuring the peak intensity of the fluorescence, and a linear curve was observed in the range of 5–1000 U/ml CA-125, which is suitable for quantitative work. The linear equation is y = 1.422x+712.75 R^2=0.9516 (Figure 5), where the CA-125 concentration (x) is measured in U/mL, and y denotes the absorbance (absorbance intensity). To determine the dynamic concentration range for the optical assay, we used a series of CA-125 concentrations ranging from 5 to 5000 U mL-1 along with optimum concentrations of mAb. Ab-QDs were utilized to introduce the optical assay's dynamic range concentration. A linear curve was created based on the mean of three independent experiments. Specifically, no less than 20 observations were used to generate the blank signal without antigen to compute reliable results for the standard deviation (0.017).

To determine the limit of detection (LOD), we used the formula OD at LOD ¼ OD mean blk + 1.645SDblk. The estimated LOD was 4.5 U mL-1. This value is similar to that gotten using the current commercial method for CA-125 .[43] [44]. This finding confirmed this method's capability to identify CA-125 in a broad range of concentrations, making it a valuable tool for early cancer detection.

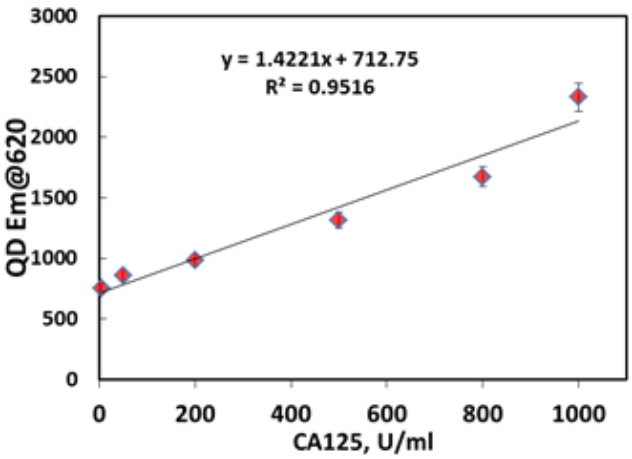

Figure 5. Detection of different concentrations of CA-125 using Ab with QDs.

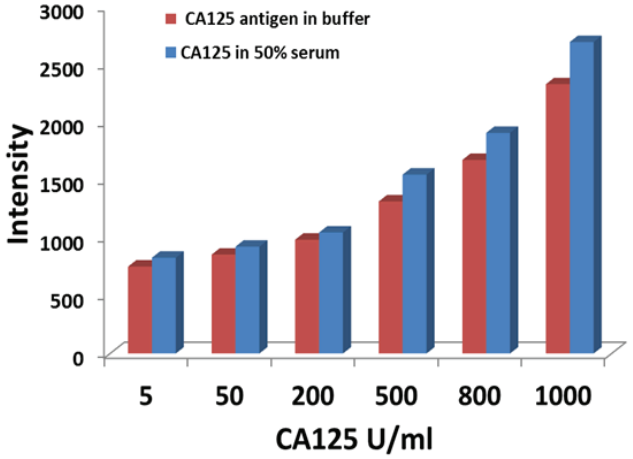

Figure 6. Comparison of CA-125 detection by QD-labeled Ab in the presence and absence of 50% human serum.

CA-125 Test in the Presence of Human Serum

The interference detection experiment was performed to rule out the potential for interference from human serum. To test the influence of antigen concentration on CA-125 detectability, human serum was mixed with a known amount of the substance. There was no discernible signal change when human serum was present, as seen in Figure (6). The assay can be run in a diluted matrix without significantly impacting the signal.

CONCLUSION

This study used a reaction technique with sequential ion layer adsorption to produce CdSe QDs that are generally uniform in size. With uniform crystallinity and homogeneous size distributions, the assembled CdSe QDs nanocrystal cores displayed a wide array of nonlinear properties under transmission electron microscopy (TEM), such as self-defocusing, two-photon absorption, and non-saturable absorption. Labeling the ovarian cancer biomarker CA-125 with quantum dots allowed the successful detection of serum antigen CA-125 by optical emission at 620 nm. The assay demonstrated a broad dynamic range for CA-125 concentrations. There was a detection limit of 4.5 U mL-1. Despite this, the assay worked reasonably well with the various biological components contained in 50% human serum, and there were no discernible alterations in the results.

AUTHORSHIP CONTRIBUTIONS

Authors equally contributed to this work.

DATA AVAILABILITY STATEMENT

The authors confirm that the data that supports the findings of this study are available within the article. Raw data that support the finding of this study are available from the corresponding author, upon reasonable request.

CONFLICT OF INTEREST

The author declared no potential conflicts of interest with respect to the research, authorship, and/or publication of this article.

ETHICS

There are no ethical issues with the publication of this manuscript.

REFERENCES

[1] Khazaei Z, Namayandeh SM, Beiranvand R, Naemi H, Bechashk SM, Goodarzi E. Worldwide incidence and mortality of ovarian cancer and Human Development Index (HDI): GLOBOCAN sources and methods 2018 J Prev Med Hyg 2021;62:E174.

[2] Momenimovahed Z, Tiznobaik A, Taheri S, Salehiniya H. Ovarian cancer in the world: epidemiology and risk factors. Int J Womens Health 2019;11:287–299. [CrossRef]

[3] Reid BM, Permuth JB, Sellers TA. Epidemiology of ovarian cancer: a review. Cancer Biol Med 2017;14:9. [CrossRef]

[4] DiSaia PJ, Creasman WT, Mannel RS, McMeekin DS, Mutch DG. Clinical gynecologic oncology e-book. Elsevier Health Sciences; 2017.

[5] Elias KM, Guo J, Bast RC. Early detection of ovarian cancer. Hematol Clin 2018;32:903–914. [CrossRef]

[6] Nersesian S, Glazebrook H, Toulany J, Grantham SR, Boudreau JE. Naturally killing the silent killer: NK cell-based immunotherapy for ovarian cancer. Front Immunol 2019;10:1782. [CrossRef]

[7] Konstantinopoulos PA, Norquist B, Lacchetti C, Armstrong D, Grisham RN, Goodfellow PJ, et al. Germline and somatic tumor testing in epithelial ovarian cancer: ASCO guideline. J Clin Oncol 2020;38:1222. [CrossRef]

[8] Zeff N. Role of laparoscopy in initial tumor staging in advanced epithelial ovarian cancer: a systematic review. Pleura Peritoneum 2018;3:20180106. [CrossRef]

[9] Landegren U, Hammond M. Cancer diagnostics based on plasma protein biomarkers: hard times but great expectations. Mol Oncol 2021;15:1715–1726. [CrossRef]

[10] Cvetkovic D. Early events in ovarian oncogenesis. Reprod Biol Endocrinol 2003;1:1–7. [CrossRef]

[11] Reiter MJ, Costello JE, Schwope RB, Lisanti CJ, Osswald MB. Review of commonly used serum tumor markers and their relevance for image interpretation. J Comput Assist Tomogr 2015;39:825–834. [CrossRef]

[12] Gubbels JAA, Claussen N, Kapur AK, Connor JP, Patankar MS. The detection, treatment, and biology of epithelial ovarian cancer. J Ovarian Res 2010;3:1–11. [CrossRef]

[13] Charkhchi P, Cybulski C, Gronwald J, Wong FO, Narod SA, Akbari MR. CA125 and ovarian cancer: a comprehensive review. Cancers (Basel) 2020;12:3730. [CrossRef]

[14] Twickler DM, Moschos E. Ultrasound and assessment of ovarian cancer risk. Am J Roentgenol 2010;194:322–329. [CrossRef]

[15] Malati T. Tumour markers: an overview. Indian J Clin Biochem 2007;22:17–31. [CrossRef]

[16] National Cancer Institute. Cancer and Nanotechnology - NCI. 2022. Available at: https://www.cancer.gov/nano/cancer-nanotechnology Last Accessed. Date: 22.11.2024

[17] Allayla AMT, Faris RA, Mahdi ZF. Construction of insulin-like growth factor nanocomposite biosensor by Raman spectroscopy. Vib Spectrosc 2021;114:103252. [CrossRef]

[18] Faris RA, Mahdi ZF, Husein MDA. Immobilised gold nanostructures on printing paper for label-free surface-enhanced Raman spectroscopy. IOP Conf Ser Mater Sci Eng 2020;871:12019. [CrossRef]
[19] Faris RA, Mahdi ZF, Al-Layla AMT. Preliminary study of the insulin growth factor binding protein-3 (IGFBP3) level in Iraqi women with breast cancer. AIP Conf Proc 2021;2372:30003. [CrossRef]
[20] Mahdi ZF, Faris RA, Sadeq ZS. Fast, sensitive and low-cost chemical sensor based on manufacturing nanostructured Co3O4 using Raman spectroscopy. Nano-Struct Nano-Obj 2021;28:100778. [CrossRef]
[21] Michalet X, Pinaud FF, Bentolila LA, Tsay JM, Doose S, Li JJ, et al. Quantum dots for live cells, in vivo imaging, and diagnostics. Science 2005;307:538–544. [CrossRef]
[22] Gokarna A, Jin LH, Hwang JS, Cho YH, Lim YT, Chung BH, et al. Quantum dot-based protein micro- and nanoarrays for detection of prostate cancer biomarkers. Proteomics 2008;8:1809–1818. [CrossRef]
[23] Marchal F, Pic E, Pons T, Dubertret B, Bolotine L, Guillemin F. Quantum dots in oncological surgery: the future for surgical margin status? Bull Cancer 2008;95:1149–1153.
[24] Weng KC, Noble CO, Papahadjopoulos-Sternberg B, Chen FF, Drummond DC, Kirpotin DB, et al. Targeted tumor cell internalization and imaging of multifunctional quantum dot-conjugated immunoliposomes in vitro and in vivo. Nano Lett. 2008;8(9):2851–2857. [CrossRef]
[25] Zhou M, Ghosh I. Quantum dots and peptides: a bright future together. Pept Sci 2007;88:325–339. [CrossRef]
[26] Erogbogbo F, Yong KT, Roy I, Xu G, Prasad PN, Swihart MT. Biocompatible luminescent silicon quantum dots for imaging of cancer cells. ACS Nano 2008;2:873–878. [CrossRef]
[27] Ben-Ari ET. Nanoscale quantum dots hold promise for cancer applications. J Natl Cancer Inst 2003;95:502–504. [CrossRef]
[28] Hezinger AFE, Teßmar J, Göpferich A. Polymer coating of quantum dots: a powerful tool toward diagnostics and sensorics. Eur J Pharm Biopharm 2008;68:138–152. [CrossRef]
[29] Yong KT, Roy I, Swihart MT, Prasad PN. Multifunctional nanoparticles as biocompatible targeted probes for human cancer diagnosis and therapy. J Mater Chem 2009;19:4655–4672. [CrossRef]
[30] Smith AM, Dave S, Nie S, True L, Gao X. Multicolor quantum dots for molecular diagnostics of cancer. Expert Rev Mol Diagn 2006;6:231–244. [CrossRef]
[31] Zhang H, Yee D, Wang C. Quantum dots for cancer diagnosis and therapy: biological and clinical perspectives. Nanomedicine (Lond) 2008;3:83–91. [CrossRef]
[32] Smith AM, Duan H, Mohs AM, Nie S. Bioconjugated quantum dots for in vivo molecular and cellular imaging. Adv Drug Deliv Rev 2008;60:1226–1240. [CrossRef]
[33] Tada H, Higuchi H, Wanatabe TM, Ohuchi N. In vivo real-time tracking of single quantum dots conjugated with monoclonal anti-HER2 antibody in tumors of mice. Cancer Res 2007;67:1138–1144. [CrossRef]
[34] Shah BS, Clark PA, Moioli EK, Stroscio MA, Mao JJ. Labeling of mesenchymal stem cells by bioconjugated quantum dots. Nano Lett 2007;7:3071–3079. [CrossRef]
[35] Yong KT, Ding H, Roy I, Law WC, Bergey EJ, Maitra A, et al. Imaging pancreatic cancer using bioconjugated InP quantum dots. ACS Nano 2009;3:502–510. [CrossRef]
[36] Fang M, Peng C, Pang DW, Li Y. Quantum dots for cancer research: current status, remaining issues, and future perspectives. Cancer Biol Med 2012;9:151.
[37] Khaledian S, Abdoli M, Fatahian R, Zahabi SS. Quantum dots in cancer cell imaging. In: Quantum Dots-Recent Advances, New Perspectives and Contemporary Applications. London: IntechOpen; 2023. [CrossRef]
[38] Liang Z, Khawar MB, Liang J, Sun H. Bio-conjugated quantum dots for cancer research: detection and imaging. Front Oncol 2021;11:749970. [CrossRef]
[39] Jaffar AF, Salman AM, Akram IN, Al Dergazly AA. Nonlinear properties and optical limiting of olive oil by using z-scan technique. Al- Nahrain University; 2012. [CrossRef]
[40] Salman AM, Salman AA, Al-Janabi A. Stable L-band multiwavelength erbium-doped fiber laser based on four-wave mixing using nickel nanofluid. Appl Opt 2019;58:6136–6143. [CrossRef]
[41] Xu P, Feng W, Wang M, Zhang L, Liang G, Jing A. New ultrasensitive sandwich-type immunoassay of dendritic tri-fan blade-like PdAuCu nanoparticles/amine-functionalized graphene oxide for label-free detection of carcinoembryonic antigen. Micromachines 2021;12. [CrossRef]
[42] Al-Ogaidi I, Aguilar ZP, Suri S, Gou H, Wu N. Dual detection of cancer biomarker CA125 using absorbance and electrochemical methods. Analyst 2013;138:5647–5653. [CrossRef]
[43] Li JJ, et al. Large-scale synthesis of nearly monodisperse CdSe/CdS core/shell nanocrystals using air-stable reagents via successive ion layer adsorption and reaction. J Am Chem Soc 2003;125:12567–12575. [CrossRef]
[44] Mongia SK, Rawlins ML, Owen WE, Roberts WL. Performance characteristics of seven automated CA125 assays. Am J Clin Pathol 2006;125:921–927. [CrossRef]